CRYSTAL GROWTH & DESIGN

Article

pubs.acs.org/crystal

A Route to Bimodal Micro-Mesoporous Metal–Organic Frameworks Nanocrystals

Minh-Hao Pham,[†] Gia-Thanh Vuong,[†] Frédéric-Georges Fontaine,[‡] and Trong-On Do*[,†]

[†]Department of Chemical Engineering, and [‡]Department of Chemistry, Centre de Recherche sur les Interfaces et la Catalyse (CERPIC), Laval University, Quebec, G1V 0A6, Canada

Supporting Information

ABSTRACT: To overcome the pore size constraints (pore size < 2 nm) of crystalline microporous metal–organic frameworks (MOFs), one can either reduce crystal size or create mesopore channels in the MOF crystals. Our approach does both, using a solvothermal nonionic surfactant-templated assembly of microblocks in the presence of acetic acid, which not only generates well-defined mesopore channels within the microporous MOF nanocrystals but also gives high crystallinity. Two examples were selected to illustrate our approach using $[Cu_3(BTC)_2]$- and $[Cu_2(HBTB)_2]$-based MOFs (H_3BTC = 1,3,5-benzenetricarboxylic acid; H_3BTB = 1,3,5-Tris[4-carboxyphenyl]benzene).

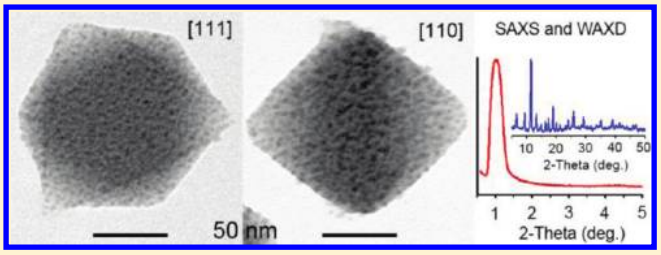

INTRODUCTION

Crystalline metal–organic frameworks (MOFs), constructed from the assembly of organic linkers with metal ions or metal clusters, are scaffoldings with all or most atoms on internal surfaces, which leads to exceptionally high surface areas (up to 6500 $m^2\ g^{-1}$) and pore volumes (up to 3.6 $cm^3\ g^{-1}$).[1−3] They have emerged as an important new class of materials with a significant impact in molecular separation, gas storage, catalysis, sensing, and drug delivery.[1,4a−c] Although MOFs exhibit very large surface areas, the microporosity of these materials (pore size < 2 nm) restrains the accessibility of a significant portion of the surface area to large guests, which limits their potential applications. Therefore, to upgrade the performance of these materials, attempts have been made to synthesize porous materials with large pore diameters in the 2−50 nm range.[2,3,5] For example, MIL-101,[2] UMCM-2,[3] and PCN-105[5b] exhibit mesoporous behavior owing to mesoporous cages found throughout the structure; however, the mesopores are often restricted by small apertures that prohibit large molecules from accessing the space inside. Increasing the organic linker length is another option, but, with few exceptions,[1,6] the MOFs built up from long-linkers tend to collapse upon guest removal[7] or form catenated structures.[8] As in the case of microporous zeolites,[9,10] materials with bimodal micro-/mesoporosity are of considerable interest for many potential applications, such as drug release, gas storage, separation, and catalysis because they offer the benefits arising from the combined two regimes.[10,11] However, no rational synthetic procedure to incorporate mesopores in MOFs that can be applied to a large array of carboxylate-based MOFs has yet been reported.[12] We report here a novel methodology toward the synthesis of a new family of bimodal micro-mesoporous MOF nanocrystals via the coassembly of nanosized MOF building blocks with a nonionic triblock copolymer surfactant in the presence of acetic acid. The use of a large triblock copolymer surfactant such as F127 ($EO_{97}PO_{69}EO_{97}$) as a mesostructured template induces the ability to crystallize a MOF structure of pore walls, while the presence of acetic acid allows controlling the rate of crystallization of the framework to form well-defined mesostructures within the crystalline MOF nanocrystals.

EXPERIMENTAL SECTION

Chemicals. CH_3COOH (99.7%, Fisher), Pluronic F127 ($EO_{97}PO_{69}EO_{97}$, average $M_n \sim 12\,600$, Aldrich), 1,3,5-benzenetricarboxylic acid (H_3BTC, 95%, Aldrich), 1,3,5-tris(4-carboxyphenyl)-benzene (H_3BTB, ≥ 98%, Aldrich), $Cu(NO_3)2{\cdot}3H_2O$ (≥99%, Aldrich), and anhydrous ethanol as solvent were purchased from commercial sources and used without further purification.

Synthesis. Bimodal micro-mesoporous MOFs nanocrystals were prepared by using a solvothermal synthesis in the presence of triblock copolymer F127 as the template and acetic acid with various molar ratios of acetic acid/Cu^{2+} in ethanol. In a typical synthesis of bimodal micro-mesoporous $[Cu_3(BTC)_2]$ based MOFs, namely, UL1MOF-*x*, 0.618 mL (10.8 mmol) of acetic acid was added to a 6 mL ethanol solution containing 0.435 g (1.8 mmol) of $Cu(NO_3)_2{\cdot}3H_2O$. To this solution, 0.216 g of F127 surfactant predissolved in 6 mL of ethanol was added. After stirring for 2 h, 0.221 g (1.0 mmol) of H_3BTC was added. After stirring for an additional 2 h, the reaction mixtures were heated at 120 °C for 16 h. The product was washed several times with ethanol, recovered by centrifugal separation, and then dried at 70 °C for 4 h. To remove the surfactant, the products were treated with tetrahydrofuran (THF) in the presence of acetic acid as solvent (molar ratio acetic acid/THF = 0.15/1.0) with the ratio of 1 g of the material for 400 mL of the solvent at 100 °C for 24 h. The same procedure was

Received: November 10, 2011
Revised: December 1, 2011
Published: December 7, 2011

ACS Publications © 2011 American Chemical Society

dx.doi.org/10.1021/cg201483y | *Cryst. Growth Des.* 2012, 12, 1008–1013

used for the synthesis of bimodal [$Cu_2(HBTB)_2$] based MOFs, namely, UL2MOF-*x*, except that H_3BTB was used as linkers instead of H_3BTC, with the molar ratio of $Cu(NO_3)_2{\cdot}3H_2O$/0.28 H_3BTB/33 CH_3COOH/0.05 F127/620 C_2H_5OH, at 110 °C for 16 h.

Characterization. Powder X-ray diffraction (XRD) patterns in the 2θ range of 0.5−5° for small-angle X-ray scattering (SAXS) and 5−50° for wide-angle X-ray diffraction (WAXD) were collected on a Bruker SMART APEX II X-ray diffractometer equipped with Cu K_α radiation (40 kV, 30 mA). Scanning electron microscopy (SEM) images were taken with a JEOL 6360 instrument with an accelerating voltage of 3 kV. Transmission electron microscopy (TEM) images were obtained with a 120 kV JEOL JEM 1230 electron microscope. High resolution transmission electron microscopy (HRTEM) investigations were carried out on a JEOL JEM-2100F electron microscope operating at 200 kV (point resolution 0.1 nm). N_2 adsorption−desorption isotherms were measured at the temperature of liquid nitrogen with a Quantachrome Autosorb-1 system. The BET surface areas were calculated from the experimental pressure ranges identified by established consistency criteria reported by Walton and Snurr for metal−organic frameworks,[13] herein the 0.05−0.15 P/P_0 range of linearity of the adsorption isotherm. The pore size distributions were obtained from the analysis of the desorption branch of the isotherms using the BJH model. Thermogravimetric analysis/differential thermal analysis (TGA/DTA) was carried out with a Netzsch STA 449C thermal analysis instrument from room temperature to 500 °C with a heating rate of 5 °C min^{-1} under an air flow of 20 mL min^{-1} using the Netzsch Proteus data analysis package. The elemental analysis of carbon and copper was performed using a Perkin-Elmer 240C elemental analyzer and a Perkin-Elmer Analyst 200 Atomic Absorption spectrometer, respectively.

RESULTS AND DISCUSSION

A typical mixture for the synthesis of the bimodal micro-mesoporous nanomaterials (namely, ULMOF-*x*; *x* = acetic acid/Cu^{2+} molar ratio) is composed of acetic acid (AA), copper(II) nitrate trihydrate, and nonionic triblock copolymer surfactant (Pluronic F127). The solution was stirred for 2 h before the carboxylate linker was added (H_3BTC for UL1MOF-*x* or H_3BTB for UL2MOF-*x*) and was followed by a solvothermal treatment. The crystals obtained were extracted with tetrahydrofuran in the presence of acetic acid to remove the surfactant.

Figure 1 shows the SAXS and WAXD patterns for the as-made UL1MOF-*x* samples obtained from different acetic acid to Cu(II) molar ratios (AA/Cu^{2+} = 0, 4, and 6) in the presence of Pluronic F127 and H_3BTC, and for pristine $Cu_3(BTC)_2$ (HKUST-1)[14] as well, as prepared by Hartmann et al. using the same copper starting material.[15] The presence of a single d_{100} peak in the SAXS spectra for the materials prepared in the presence of acetic acid and F127 suggests a disordered wormhole-like mesostructure.[10,16] This peak grows in intensity and shifts from 1.4° to 1.1° when the AA/Cu^{2+} molar ratio is increased from 0 to 6, suggesting a more uniform mesostructure and larger d_{100} for these materials. It is important to note that using an AA/Cu^{2+} ratio of 12, under the same synthetic conditions, does not alter significantly the intensity and the position of the d_{100} peak, indicating that a similar mesostructure is obtained for this sample (Supporting Information, Table S1). As expected, no d_{100} peak is present for the pristine HKUST-1 material since it possesses no mesopores. A comparison of the WAXD of UL1MOF-6 samples with pristine HKUST-1 sample confirms that both materials have the same microcrystalline network.[15] However, the broad diffraction peaks indicate that UL1MOF-6 is composed of small nanocrystals. By considering the pristine HKUST-1 to be 100% crystalline, the crystallinity of the

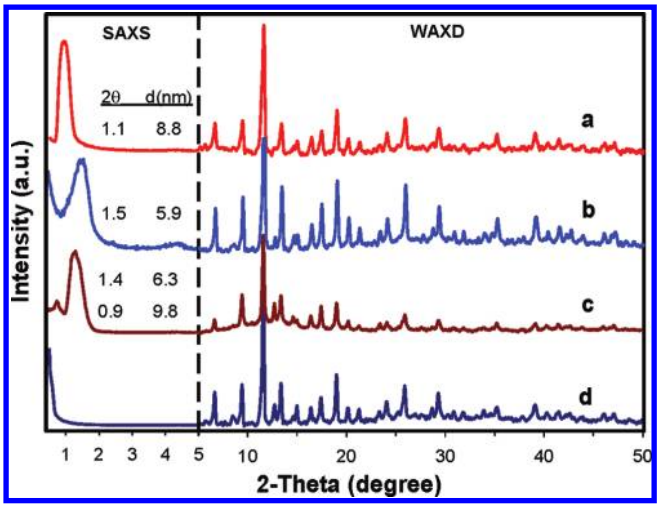

Figure 1. Powder XRD patterns for UL1MOF-*x*. SAXS (left) and WAXD (right) patterns for the as-made UL1MOF-*x* obtained from various molar ratios of acetic acid/Cu^{2+}: (a) *x* = 6, (b) *x* = 4, (c) *x* = 0, and (d) the pristine $Cu_3(BTC)_2$ MOF. UL1MOF-*x* were synthesized with a molar ratio of $Cu^{2+}/H_3BTC/CH_3COOH/C_2H_5OH$: F127 = 1: 0.56: *x*: 115: 0.01 at 120 °C for 16 h.

samples UL1MOF-0, -2, -4, -6, and -12 was determined to be 58, 85, 89, 94, and 92% crystalline, respectively.[17] All these results suggest that higher crystallinity and more uniform wormhole-like mesostructure are obtained for UL1MOF-*x* by increasing the AA/Cu^{2+} molar ratio. It emphasizes the key role of acetic acid in the formation of both the micropore and well-defined mesopore structures within the MOF nanocrystals.

The nitrogen adsorption/desorption isotherm at 77 K of the solvent-extracted UL1MOF-6 is presented in Figure 2. Data for

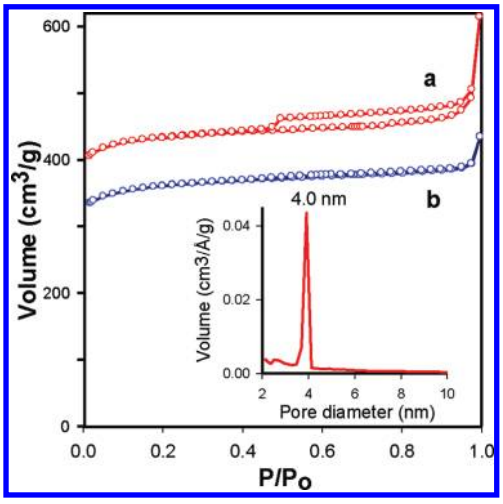

Figure 2. N_2 adsorption−desorption isotherms: (a) the solvent-extracted UL1MOF-6 displays a type I isotherm at relatively low P/P_0 pressures for a micropore structure and a typical type IV isotherm with a H_4 hysteresis loop associated with mesopore channels (inset: the mesopore diameter distribution for the UL1MOF-6), (b) the pristine $Cu_3(BTC)_2$ exhibits a type I isotherm characterizing a micropore structure with a smaller pore volume.

the pristine HKUST-1 sample are included for comparison. The latter material displays a type I isotherm at relatively low P/P_0 pressures, which is characteristic of the micropore structure, with BET surface area and pore volume of 1420

dx.doi.org/10.1021/cg201483y | Cryst. Growth Des. 2012, 12, 1008−1013

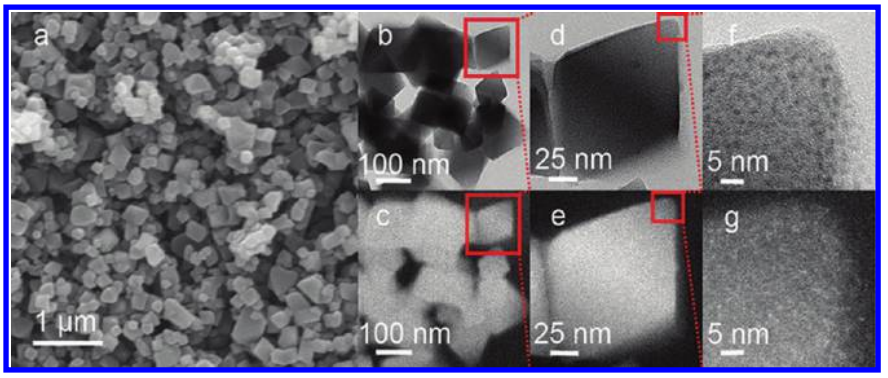

Figure 3. Electron microscopy images of UL1MOF-6. (a) SEM image showing the isolated octahedral mesoporous MOF crystals with the size in a range of 100−200 nm, (b, d, f) bright-field HRTEM images with different magnifications indicating a three-dimensional wormhole-like mesostructure, (c, e, g) dark-field HRTEM images obtained on the same area of the sample. The bright spots in the dark-field images correspond to MOF nanocrystal building blocks.

m^2 g^{-1} and 0.60 cm^3g^{-1}, respectively. However, for the UL1MOF-6 sample, in addition to the type I isotherm indicative of a microporous structure with a diameter of 8.5 Å, as in pristine HKUST-1 (ESI, Figure S1), a typical type IV isotherm with a H_4 hysteresis loop at relatively high P/P_0 (P/P_0 = 0.4−0.9) was observed. This is related to the capillary condensation associated with mesopore channels, indicating the presence of an additional mesoporous structure in this sample. The adsorption/desorption isotherms in Figure 2 are nearly horizontal and parallel over a wide range of P/P_0. This loop type is associated with uniform mesopores of the extracted UL1MOF-6.[18] The total surface area (BET surface area = 1630 m^2 g^{-1}) and pore volume (0.79 cm^3 g^{-1}) of UL1MOF-6 are comprised of both types of pores and are significantly higher than those obtained for the HKUST-1 sample, due to the presence of the mesostructure. The mesopore diameter distribution was calculated using the Barrett−Joyner−Halenda (BJH) method (inset of Figure 2), indicating a narrow mesopore diameter distribution with an average value of 4.0 nm. This mesopore diameter is also comparable to the known value for the mesoporous SBA-16 silica synthesized using the same F127 surfactant.[19] This also indicates that the ordered mesostructure is still preserved after the removal of surfactant molecules from this UL1MOF-6 sample.

The SEM image of the UL1MOF-6 sample shows the overall octahedral morphology of $[Cu_3(BTC)_2]$-based MOF produced by our procedure (Figure 3a). The discrete octahedral nanocrystals do not aggregate and exhibit a uniform crystal size ranging from 100 to 200 nm. Representative TEM images of the UL1MOF-6 show similar morphology (Figure 3b,c and Supporting Information, Figure S2) to that of the micrometer-sized HKUST-1 single crystals obtained by the original procedure (Supporting Information, Figure S3).[14,15] Indeed, the bipyramidal hollow octahedrons are clearly observed using TEM images with different views (Figure 4). For the characterization of mesopore-ordered framework consisting of crystalline nanoparticle domains, bright/dark-field high resolution-TEM images were recorded on the same area to substantiate claims of high crystallinity and mesoporosity on this material.[20] Shaped octahedral crystals were clearly observed (Figure 3d,e), and Figure 3f,g reveal a quite uniform pore size with a disordered mesopore structure, which is consistent with the SAXS results and reminiscent of MSU-1[16] and UL-zeolite,[10] which have wormhole-like mesopore structures. The bright spots in the dark-field and the dark spots in the bright-field HRTEM image (Figure 3g,f, respectively) correspond to continuous small MOF nanocrystals within the well-defined octahedron. All these results suggest that the octahedral mesocrystals are constructed from nanometric crystallites which are embedded along the organic hydrophilic block from the surfactant chains to form crystalline mesopore walls, while preserving the mesostructural integrity. Note that these MOF samples are quite sensitive to the electron beam compared to other mesostructured metal oxides obtained with F127 as a structure-directing agent and makes it challenging to obtain selected-area electron diffraction patterns.[21]

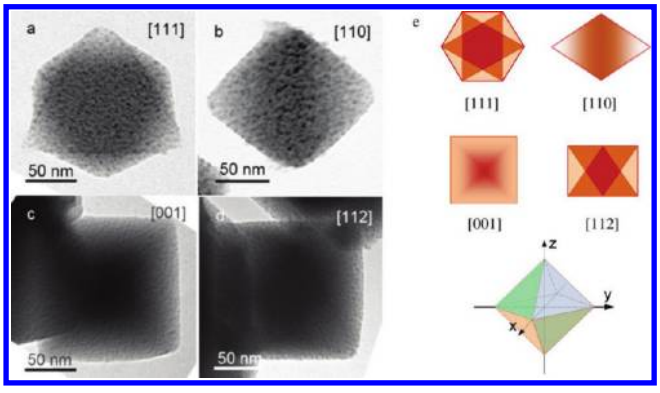

Figure 4. (a−d) TEM images recorded along different directions: (a) along the [111] direction, (b) along the [110] direction, (c) along the [001] direction, and (d) along the [112] direction. (e) Schematic representations of the TEM images, and the octahedral reconstructed three-dimensional shape of a UL1MOF-6 nanocrystal.

TGA-DTA measurements for the as-synthesized and extracted-UL1MOF-6 materials were carried out under air flow (Supporting Information, Figure S4). For the extracted-UL1MOF-6 sample, the TGA-DTA profile shows a weight loss of ∼10% at below 180 °C that can be attributed to the solvent desorption within the pore channels of the extracted sample. However, no significant weight loss (< 5%) was found for the UL1MOF-6 sample before extraction suggesting an F127 template inside the mesopore structure. Furthermore, no essential difference in the thermal stability between materials was observed; their structure is thermally stable up to 280 °C. In the temperature range of 250−350 °C, because of a

dx.doi.org/10.1021/cg201483y | Cryst. Growth Des. 2012, 12, 1008−1013

simultaneous decomposition of the F127 template[22] and the MOF structure of UL1MOF-6, it is difficult to identify one from the other. However, the weight loss of the as-synthesized UL1MOF-6 (59%) in the range of 280−330 °C is greater than that of extracted UL1MOF-6 (51%), implying the presence of the F127 copolymer in the as-made sample. The FTIR spectra of these samples are also identical (Supporting Information, Figure S5). In addition, C and Cu elemental analysis was also performed. The atomic ratio of C to Cu of the UL1MOF-6 before surfactant extraction is 9.5, which is higher than those of the UL1MOF-6 after surfactant extraction (C/Cu = 7.8) and as compared to those of the pristine HKUST-1 (C/Cu = 7.6). This clearly indicates the presence of surfactant F127 inside mesopore channels of the UL1MOF-6 nanocrystals before extraction.

The same procedure was also applied successfully for the synthesis of $[Cu_2(HBTB)_2]$-based MOF mesocrystals (namely, UL2MOF-*x*) using H_3BTB as the linker instead of H_3BTC. Figure 5 shows the SAXS and WAXD patterns of the

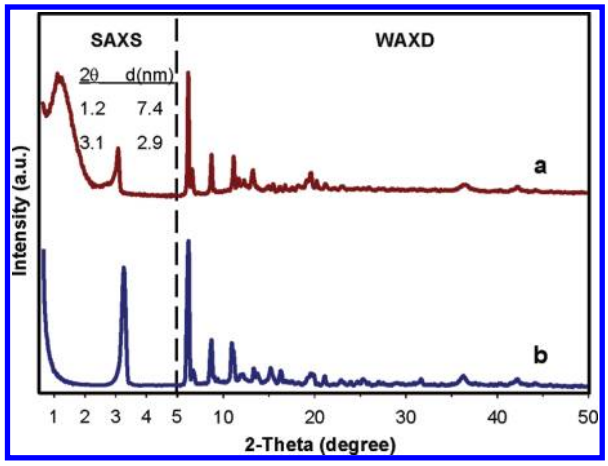

Figure 5. Powder XRD patterns for UL2MOF-6. SAXS (left) and WAXD (right) patterns for the as-made UL2MOF-6 (a) and the pristine $Cu_2(HBTB)_2$ MOF (b). UL2MOF-6 was synthesized using H_3BTB as the organic linker and a molar ratio $Cu^{2+}/H_3BTB/CH_3COOH/C_2H_5OH/F127$ = 1: 0.28: 33: 620: 0.05 at 110 °C for 16 h.

$[Cu_2(HBTB)_2]$ based MOF prepared with the same surfactant and acetic acid concentrations in the synthetic solution (AA/Cu^{2+} = 6). For comparison, the pristine microporous $[Cu_2(HBTB)_2]$ MOF was also prepared by the method of Mu et al.[23] The SAXS patterns of all samples exhibit a diffraction peak at the 2θ value of 3.1° that is present in the pristine MOF crystal structure. For the UL2MOF-6 sample, a single d_{100} peak was observed at lower 2θ value indicating the presence of wormhole-like mesopores in this sample which is not present for the pristine sample. In addition, the nitrogen adsorption/desorption isotherm at 77 K of the UL2MOF-6 sample shows a type IV isotherm with a H_4 hysteresis loop corresponding to mesopores having a diameter of 3.9 nm (Supporting Information, Table S1).

Interestingly, this material contains numerous flower-like crystals, and almost all of them show the same morphology (Figure 6a−c). The flower-like crystals were obtained as multilamellar nanosheets with three-dimensional intergrowth. The overall thickness of the lamellar stacking is 40−60 nm. Bright-field and dark-field HRTEM images recorded on this

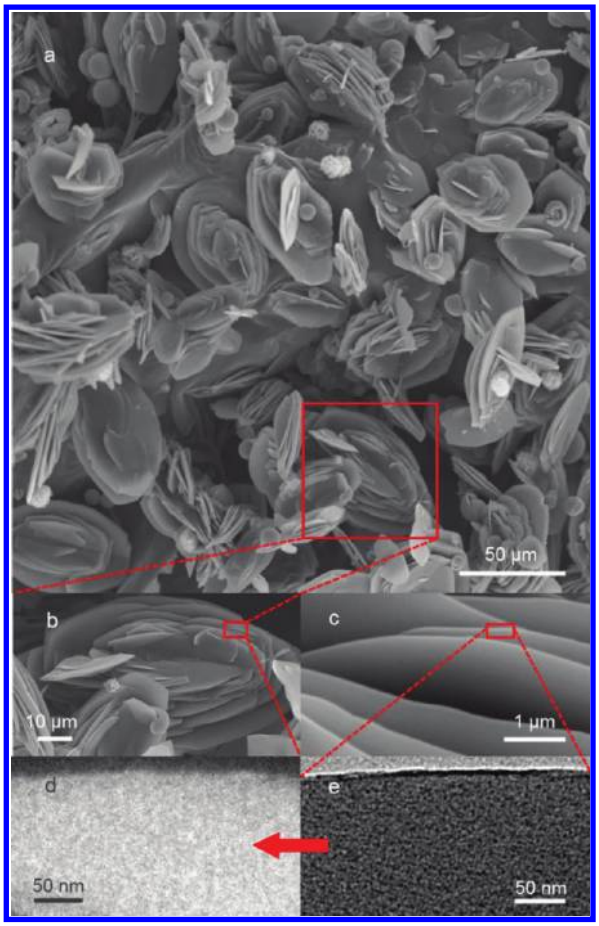

Figure 6. Electron microscopy images of UL2MOF-6 sample. (a−c) SEM images with different magnifications indicating a flower-like morphology that is composed of nanosheets, (d, e) HRTEM images of the edge of a nanosheet: (e) bright-field image showing a 3D disordered wormhole-like mesostructure, (d) dark-field image obtained on the same area of the sample shows the bright spots corresponding to MOF nanocrystal building blocks.

UL2MOF-6 sample indicate that small nanocrystals are also uniformly embedded in a continuous matrix within the crystals (Figure 6d,e). The nanocrystallite sizes are consistent with those from X-ray diffraction peak broadening. Furthermore, its crystallinity is 85% by considering the microporous $[Cu_2(HBTB)_2]$ MOF to be 100% crystalline.

On the basis of the results of this study and literature precedents, we propose a possible mechanism for the formation of bimodal MOF nanocrystals illustrated in Scheme 1. Because of the presence of acetic acid in the reaction solution containing copper(II) ions, acetate coordination species,[24] probably a derivative of the metal-acetate bidentate bridging $[Cu_2(CH_3COO)_4]$, form. Upon the addition of the linkers, nanosized building blocks including MOF components are yielded. As recently reported by Kitagawa et al. in MOF chemistry using copper(II) salt, the similar MOF building blocks with a size of a few nanometers were formed from organic linkers and acetic acid in the early stage of the reaction.[25] The nanosized building blocks here will coassemble with the surfactant micelles into mesostructures, as previously reported in the synthesis of mesoporous inorganic materials.[20] At high temperature (120 °C), the building blocks will fuse to form MOF crystals, while maintaining the mesostructure.[25−27]

dx.doi.org/10.1021/cg201483y | *Cryst. Growth Des.* 2012, 12, 1008−1013

Scheme 1. Possible Mechanism for the Formation of the Bimodal Micro-Mesoporous MOF Nanocrystals

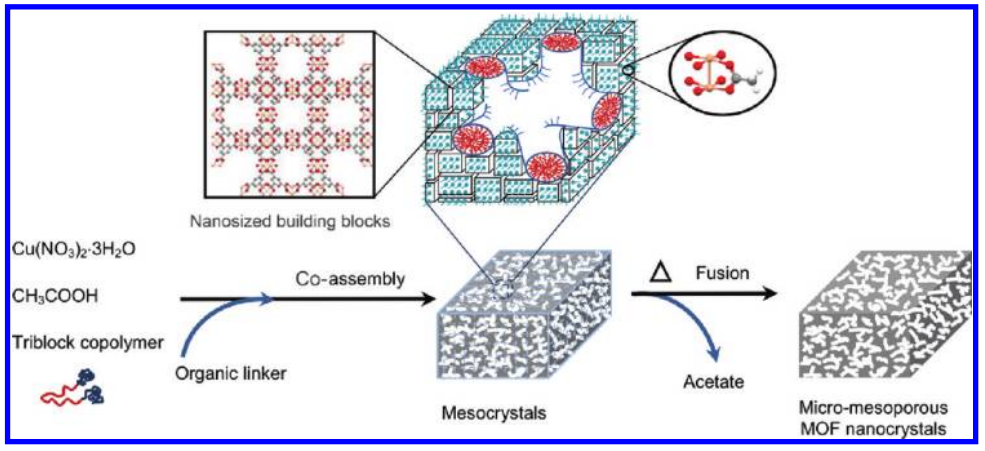

It is noted that the key factor to obtain well-defined mesoporous materials is that the growth of the framework must be slow enough for the coassembly of the nanosized building blocks and the surfactant micelles into a mesostructure to occur while avoiding phase separation.[24] Since acetic acid competes with the carboxylate linkers,[25] the growth of the framework to generate large crystals in the early stage of the reaction which can induce a phase segregation is limited. Moreover, acetic acid can also impact the deprotonation of the linkers. A higher acetic acid concentration thus leads to a lower growth rate of the MOF.[28] Therefore, by tuning the acetic acid concentration in this synthetic process, it is possible to form the well-defined mesostructures within MOF nanocrystals. The use of large triblock copolymer surfactant such as F127 in the current method allows yielding thick pore walls that induce the ability to crystallize the MOF structure to obtain highly crystalline bimodal MOF nanocrystals.[24]

CONCLUSION

To the best of our knowledge, this is the first synthesis of such bimodal MOF nanocrystals using the coassembly of nanosized MOF building blocks with a nonionic triblock copolymer surfactant in the presence of acetic acid. Bimodal ULMOF nanocrystals are considered to be of substantial scientific and technological importance, owing to easier transport of guest molecules through the mesopores, short diffusion pathways, and exposed active sites within the MOF crystals. In addition to diffusional effects, the grafting of novel functionalities within the mesopore surface by postsynthesis will also be studied, since a larger pore diameter should ease the functionalization processes.[29] We are currently looking at the synthesis of other carboxylate MOFs to establish the generality of this approach.

ASSOCIATED CONTENT

Supporting Information

Synthetic parameters and physicochemical properties of bimodal ULMOF-*x* nanocrystals (Table S1), micropore diameter distribution for the UL1MOF-6 (Figure S1), TEM images of UL1MOF-6 (Figure S2), SEM image of the pristine $Cu_3(BTC)_2$ MOF crystal (Figure S3), TGA-DTA profiles (Figure S4), and FTIR spectra (Figure S5) of the as-synthesized UL1MOFs-6, extracted-UL1MOFs-6, and pristine HKUST-1. This material is available free of charge via the Internet at http://pubs.acs.org.

AUTHOR INFORMATION

Corresponding Author

*E-mail: Trong-On.Do@gch.ulaval.ca.

ACKNOWLEDGMENTS

We thank the Natural Sciences and Engineering Research Council of Canada (NSERC), the Centre de Recherche sur les Propriétés des Interfaces et de Catalyse (CERPIC, U. Laval), and the Centre in Green Chemistry and Catalysis (CGCC, Québec) for financial support, and Vietnam Ministry of Education and Training for a scholarship (to M.H.P.). We acknowledge P. McBreen and J. D. Wuest for useful discussions.

REFERENCES

(1) (a) Yaghi, O. M.; O'Keeffe, M.; Ockwig, N. W.; Chae, H. K.; Eddaoudi, M.; Kim, J. *Nature* **2003**, *423*, 705−714. (b) Furukawa, H.; Ko, N.; Go, Y. B.; Aratani, N.; Choi, S. B.; Choi, E.; Yazaydin, A. Ö.; Snurr, R. Q.; O'Keeffe, M.; Kim, J.; Yaghi, O. M. *Science* **2010**, *329*, 424−428.

(2) Férey, G.; Mellot-Draznieks, C.; Serre, C.; Millange, F.; Dutour, J.; Surblé, S.; Margiolaki, I. *Science* **2005**, *309*, 2040−2042.

(3) Koh, K.; Wong-Foy, A. G.; Matzger, A. J. *J. Am. Chem. Soc.* **2009**, *131*, 4184−4185.

(4) (a) Horcajada, P.; Chalati, T.; Serre, C.; Gillet, B.; Sebrie, C.; Baati, T.; Eubank, J. F.; Heurtaux, D.; Clayette, P.; Kreuz, C.; Chang, J. S.; Hwang, Y. K.; Marsaud, V.; Bories, P. N.; Cynober, L.; Gil, S.; Férey, G.; Couvreur, P.; Gref., R. *Nat. Mater.* **2010**, *9*, 172−178. (b) Yanai, N.; Kitayama, K.; Hijikata, Y.; Sato, H.; Matsuda, R.; Kubota, Y.; Takata, M.; Mizuno, M.; Uemura, T.; Kitagawa, S. *Nat. Mater.* **2011**, *10*, 787−793. (c) Satoru, S.; Higuchi, M.; Matsuda, R.; Yoneda, K.; Hijikata, Y.; Kubota, Y.; Mita, Y.; Kim, J.; Takata, M.; Kitagawa, S. *Nat. Chem.* **2010**, *2*, 633−637.

(5) (a) Koh, K.; Wong-Foy, A. G.; Matzger, A. J. *Angew. Chem., Int. Ed.* **2008**, *47*, 677−680. (b) Fang, Q. R.; Yuan, D. Q.; Sculley, J.; Lu, W. G.; Zhou, H. C. *Chem. Commun.* **2012**, *48*, 254−256.

(6) Klein, N.; Semkovska, I.; Gedrich, K.; Stoeck, U.; Henschel, A.; Mueller, U.; Kaskel, S. *Angew. Chem., Int. Ed.* **2009**, *48*, 9954−9957.

(7) (a) Eddaoudi, M.; Kim, J.; Rosi, N.; Vodak, D.; Wachter, J.; O'Keeffe, M.; Yaghi, O. M. *Science* **2002**, *295*, 469−472. (b) Jiang, H.-L.; Tatsu, Y.; Lu, Z.-H.; Xu, Q. *J. Am. Chem. Soc.* **2010**, *132*, 5586−5587.

(8) Farha, O. K.; Malliakas, C. D.; Kanatzidis, M. G.; Hupp, J. T. *J. Am. Chem. Soc.* **2010**, *132*, 950−952.

(9) Vuong, G. T.; Do, T. O. *J. Am. Chem. Soc.* **2007**, *129*, 3810−3811.

(10) Do, T. O.; Kaliaguine, S. *Angew. Chem., Int. Ed.* **2001**, *40*, 3248−3251.

(11) (a) Holland, B. T.; Abrams, L.; Stein, A. *J. Am. Chem. Soc.* **1999**, *121*, 4308−4309. (b) Qiu, L. G.; Xu, T.; Li, Z. Q.; Wang, W.; Wu, Y.; Jiang, X.; Tian, X. Y.; Zhang, L. D. *Angew. Chem., Int. Ed.* **2008**, *47*, 9487−9491. (c) Zhao, Y; Zhang, J.; Han, B.; Song, J.; Li, J.; Qian Wang, Q *Angew. Chem., Int. Ed.* **2011**, *50*, 636−639. (d) Li, Y.; Zhang, D.; Guo, Y.-N.; Guan, B.; Tang, D.; Liu, Y.; Huo, Q. *Chem. Commun.* **2011**, *47*, 7809−7811.
(12) Roy, X.; MacLachlan, M. J. *Chem.—Eur. J.* **2009**, *15*, 6552−6559.
(13) Walton, K. S.; Snurr, R. Q. *J. Am. Chem. Soc.* **2007**, *129*, 8552−8556.
(14) Chui, S. S.-Y.; Lo, S. M.-F.; Charmant, J. P. H.; Orpen, A. G.; Williams, I. D. *Science* **1999**, *283*, 1148−1150.
(15) Hartmann, M.; Kunz, S.; Himsl, D.; Tangermann, O. *Langmuir* **2008**, *24*, 8634−8642.
(16) Bagshaw, S. A.; Prouzet, E.; Pinnavaia, T. J. *Science* **1995**, *269*, 1242−1244.
(17) Based on the areas of the peaks in the 2θ range of 5° to 14°.
(18) (a) Sing, K. S. W.; Everett, D. H.; Haul, R. A. W.; Moscou, L.; Pierotti, R. A.; Rouquerol, J.; Siemieniewska, T. *Pure Appl. Chem.* **1985**, *57* (No. 4), 603−619. (b) Gregg, S. J.; Sing, K. S. W. *Adsorption, Surface Area and Porosity*; Academic Press: London, 1997.
(19) Zhao, D.; Huo, Q.; Feng, J.; Chmelka, B. F.; Stucky, G. D. *J. Am. Chem. Soc.* **1998**, *120*, 6024−6036.
(20) Yang, P.; Zhao, D.; Margolese, D. I.; Chmelka, B. F.; Stucky, G. D. *Nature* **1998**, *396*, 152−155.
(21) Lebedev, O. I.; Millange, F.; Serre, C.; Van Tendeloo, G.; Férey, G. *Chem. Mater.* **2005**, *17*, 6525−6527.
(22) Jiua, J.; Kurumada, K.; Peib, L.; Tanigaki, M. *Colloids Surf., B* **2004**, *38*, 121.
(23) Mu, B.; Li, F.; Walton, K. S. *Chem. Commun.* **2009**, 2493−2495.
(24) Boettcher, S. W.; Fan, J.; Tsung, C. K.; Shi, Q.; Stucky, G. D. *Acc. Chem. Res.* **2007**, *40*, 784−792.
(25) Tsuruoka, T.; Furukawa, S.; Takashima, Y.; Yoshida, K.; Isoda, S.; Kitagawa, S. *Angew. Chem., Int. Ed.* **2009**, *48*, 4739−4743.
(26) Penn, R. L.; Banfield, J. F. *Science* **1998**, *281*, 969−971.
(27) Shekhah, O.; Wang, H.; Zacher, D.; Fischer, R. A.; Wöll, C. *Angew. Chem., Int. Ed.* **2009**, *48*, 5038−5041.
(28) Hermes, S.; Witte, T.; Hikov, T.; Zacher, D.; Bahnmuller, S.; Langstein, G.; Huber, K.; Fischer, R. A. *J. Am. Chem. Soc.* **2007**, *129*, 5324−5325.
(29) Deng, H.; Doonan, C. J.; Furukawa, H.; Ferreira, R. B.; Towne, J.; Knobler, C. B.; Wang, B.; Yaghi, O. M. *Science* **2010**, *327*, 846−850.

Supporting Information for

A Route to Bimodal Micro-Mesoporous Metal-Organic Framework Nanocrystals

Minh-Hao Pham[†], *Gia-Thanh Vuong*[†], *Frédéric-Georges Fontaine*[‡] *and Trong-On Do*[†]*

[†]Department of Chemical Engineering, [‡]Department of Chemistry, Centre de Recherche sur les Interfaces et la Catalyse (CERPIC), Laval University, Quebec, G1V 0A6, CANADA

*Corresponding author. E-mail: Trong-On.Do@gch.ulaval.ca

Table S1. Synthetic parameters and physicochemical properties of bimodal ULMOF-x nanocrystals

Sample	AA/$Cu^{2+(*)}$	F127/$Cu^{2+(*)}$	S_{BET} m^2/g	V_{pore} cm^3/g	S_{meso} m^2/g	S_{meso}/S_{BET} (%)	V_{meso} cm^3/g	S_{micro} m^2/g	V_{micro} cm^3/g	d_{meso} nm	Crystallinity %
UL1MOF-12	12	0.01	1570	0.77	300	19.1	0.29	1270	0.48	4.0	92
UL1MOF-6	6	0.01	1630	0.79	280	17.2	0.29	1350	0.50	4.0	94
UL1MOF-4	4	0.01	1105	0.64	240	21.7	0.31	865	0.33	4.0	89
UL1MOF-2	2	0.01	860	0.51	200	23.3	0.25	660	0.26	4.0	85
UL1MOF-0	0	0.01	468	0.31	148	31.6	0.18	320	0.13	4.0	58
$Cu_3(BTC)_2$	**0**	**0.00**	**1420**	**0.60**	**-**	**-**	**-**	**-**	**-**	**-**	**100**
UL2MOF-6	33	0.05	770	0.38	205	26.6	0.16	565	0.22	3.9	85
$Cu_2(HBTB)_2$	**0**	**0.00**	**586**	**0.25**	**-**	**-**	**-**	**-**	**-**	**-**	**100**

$^{(*)}$molar ratio. S_{BET} is the BET surface area. V_{pore} is the total pore volume determined by using the desorption branch of the N_2 isotherm at $P/P_0 = 0.95$. S_{meso} is the mesopore surface area estimated by subtracting S_{micro} from S_{BET}. S_{micro} and V_{micro} are the micropore surface area and micropore volume, respectively, calculated by using t-plot method. V_{meso} is the mesopore volume calculated by subtracting V_{meso} from V_{pore}. d_{meso} is the mesopore diameter determined from the local maximum of the BJH distribution of pore diameters in the desorption branch of the N_2 isotherm. The crystallinity of the samples was determined based on the areas of the peaks in the 2θ range of 5^o to 14^o by considering their respective pristine MOFs to be 100 % crystalline.

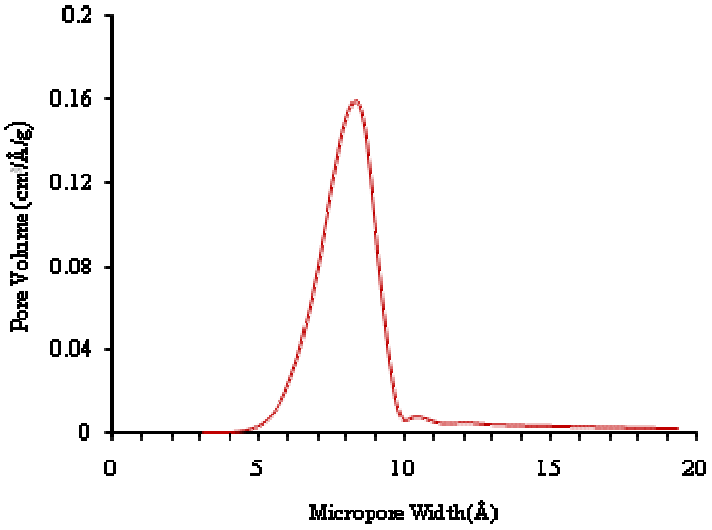

Figure S1 Micropore diameter distribution for the UL1MOF-6, using the Horvath-Kawazoe (HK) method.

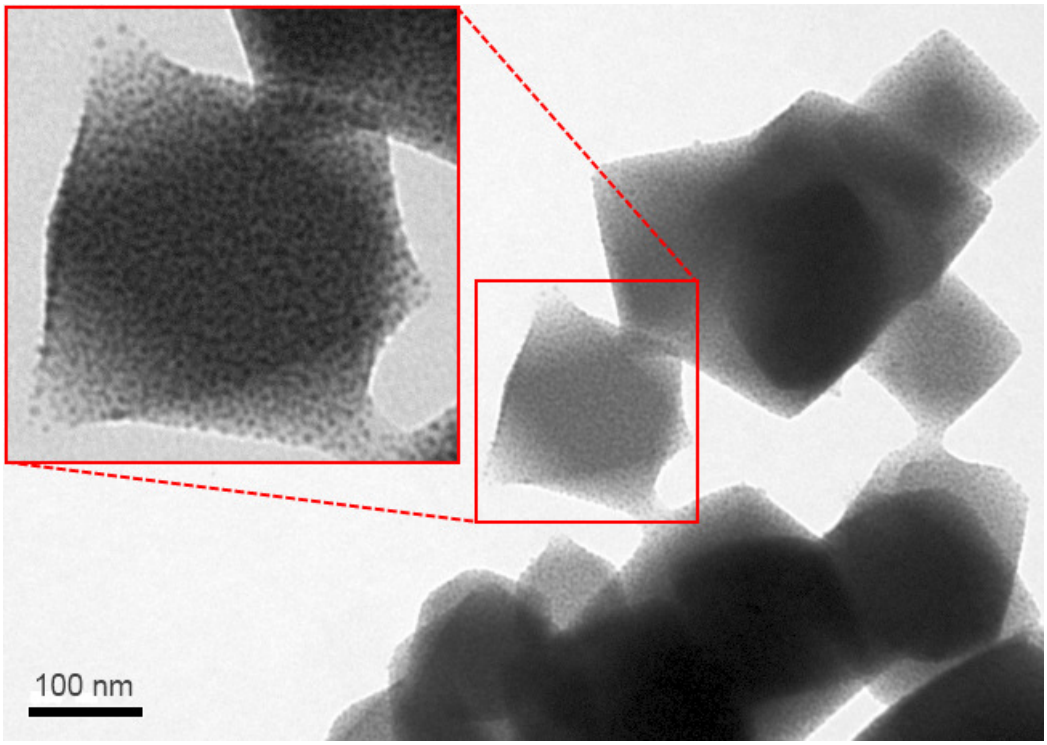

Figure S2 TEM images of UL1MOF-6 sample showing octahedral shape nanocrystals with the size in a range of 100 nm to 200 nm. These MOF nanocrystals contain a uniform three-dimensional wormhole-like mesotructure.

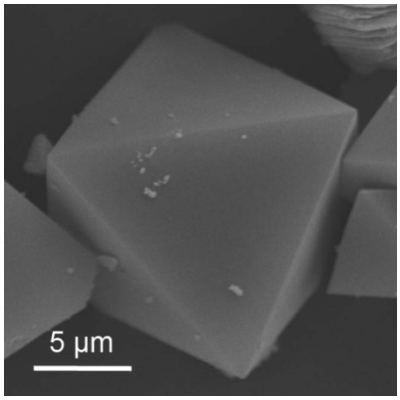

Figure S3 SEM image of the pristine microporous $Cu_3(BTC)_2$ MOF crystal prepared using the method in ref. 15. The crystal has octahedral shape with the size of 15 µm.

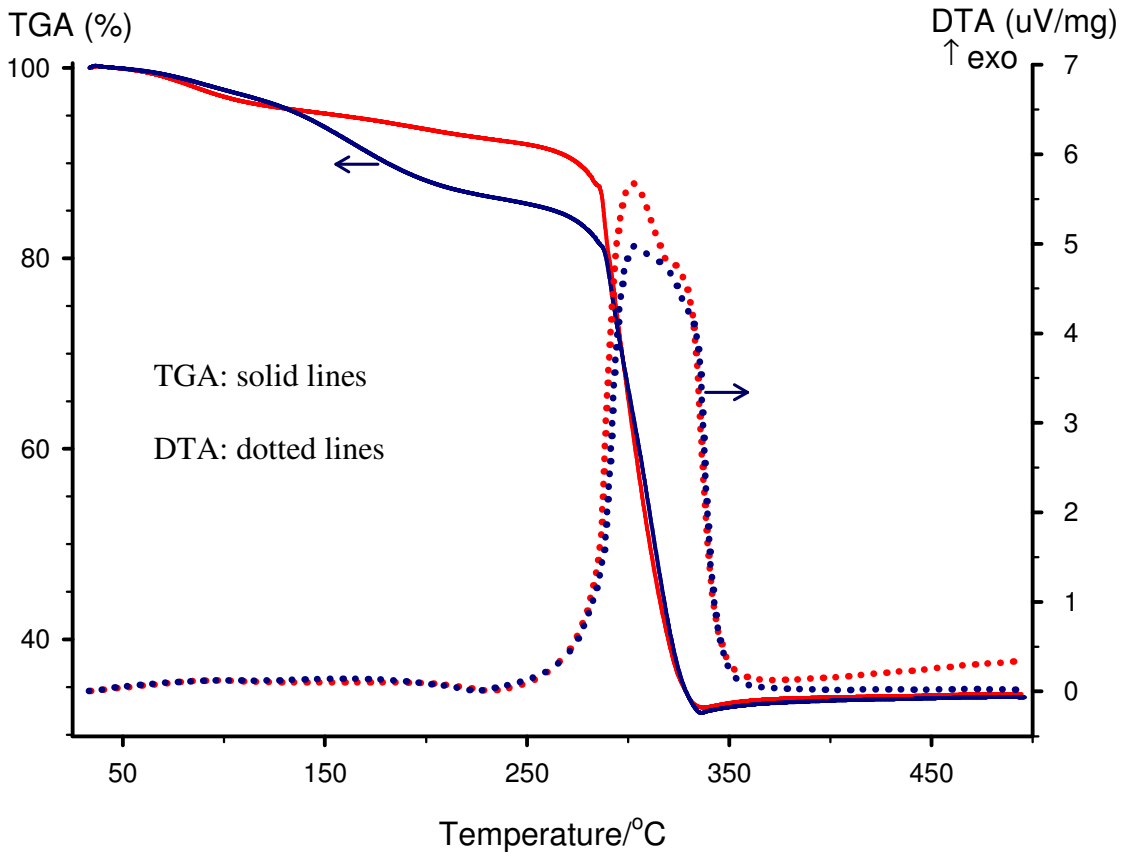

Figure S4 TGA/DTA profiles of the as-synthesized UL1MOF-6 (red) and extracted UL1MOF-6 samples (blue).

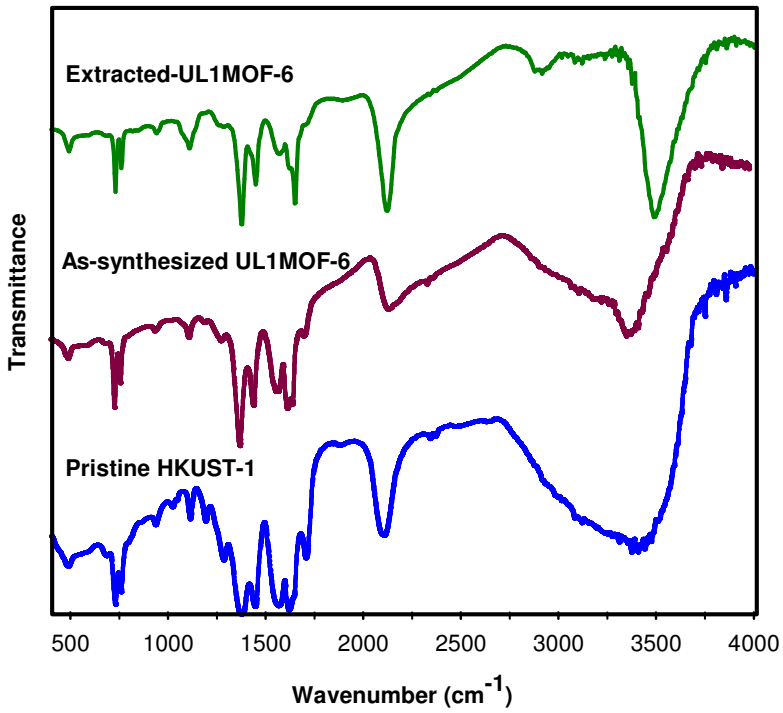

Figure S5 FTIR spectra of the as-synthesized UL1MOF-6, extracted UL1MOFs-6 and pristine HKUST-1.